AN INTEGRATIVE MODEL OF THE SELF-SUSTAINED OSCILLATING CONTRACTIONS OF CARDIAC MYOCYTES

Audrey Pustoc'h[1], Jacques Ohayon[1], Yves Usson[2], Alain Kamgoue[1] and Philippe Tracqui[1]

[1]Laboratoire TIMC, Equipe DynaCell, CNRS UMR 5525, 38706 La Tronche Cedex, France
[2]Laboratoire TIMC, Equipe RFMQ, CNRS UMR 5525, 38706 La Tronche Cedex, France

Mailing Address: Philippe Tracqui, Laboratoire TIMC, Equipe DynaCell, 38706 La Tronche Cedex, France. E-mail: Philippe.Tracqui@imag.fr

Received 22 October 2005; accepted in final form 22 October 2005

ABSTRACT

Computational cell models appear as necessary tools for handling the complexity of intracellular cell dynamics, especially calcium dynamics. However, while oscillating intracellular calcium oscillations are well documented and modelled, a simple enough virtual cell taking into account the mechano-chemical coupling between calcium oscillations and cell mechanical properties is still lacking. Considering the spontaneous periodic contraction of isolated cardiac myocytes, we propose here a virtual cardiac cell model in which the cellular contraction is modelled using an hyperelastic description of the cell mechanical behaviour. According to the experimental data, the oscillating cytosolic calcium concentrations trigger the spatio-temporal variation of the anisotropic intracellular stresses. The finite element simulations of the virtual cell deformations are compared to the self-sustained contractions of isolated rat cardiomyocytes recorded by time-lapse video-microscopy.

Key Words: calcium wave, nonlinear elasticity, CICR, mechanochemical coupling

1. INTRODUCTION

Computational biology is booming and generates many hopes in terms of public health, particularly in the domains of heart physiology (Noble, 2002). This is partly due to the fact that modelling the dynamics of complex biological phenomena by nonlinear partial differential systems is now tractable, as demonstrated by the Virtual Cell project (Slepchenko *et al.,* 2003), and amenable to a more straightforward confrontation with real data because of the increasing development of recent imaging and physical measurements techniques in living cells.

In the field of cardiac dynamics, modelling approaches started almost forty years ago and have been developed at cell, tissue and organ levels. Since the pioneering work of Fabiato and Fabiato (1975), who first measured the contractile force of isolated cardiac myocytes, study of myocardial function from analysis of single cardiac muscle cells have received an increased attention. Indeed, experiments conducted at the isolated cell

level enable an analysis of cardiomyocyte response to mechanical stress, as well as a visualisation of fast cytosolic and nuclear calcium dynamics in contracting cardiac myocytes (Ishida *et al.*, 1999).

But while mechanical stretch plays a key role in cardiac pathologies, especially cardiac hypertrophy, it remains unclear how mechanical tension is controlled and propagates intracellularly during cardiomyocytes contraction. It is known that this contraction is triggered by the mechanism of calcium-induced calcium release (CICR), a nonlinear process in which calcium liberation from the sarcoplasmic reticulum (SR) is activated by cytosolic calcium (Fabiato, 1983), due to the presence of inositol 1,4,5-triphosphate (IP_3R) receptors calcium release channels, as well as to specialized ryanodine receptor channels (RyR). In the presence of CICR, calcium influx within the cell triggers intracellular calcium release and the propagation of a calcium wave which controls the cell mechanical contraction.

Spontaneous calcium waves have been currently observed in cardiac myocytes (Ishida *et al.*, 1999), and this self-sustained dynamical behaviour has been implicated in pathologies such as cardiac arrhythmia, after-contractions, and systolic and diastolic dysfunctions (Stern *et al.*, 1988; Takamatsu and Wier, 1990; Grouselle *et al.*, 1991; Lakatta, 1992). Understanding the dynamic of the mechano-chemical couplings underlying the self-sustained contraction of isolated cardiomyocytes can be greatly facilitated by mathematical modelling of these integrated and multi-scale biochemical and biomechanical processes. However, while oscillating intracellular calcium oscillations are a well documented and modelled phenomenon (Schuster *et al.*, 2002), a precise analysis of the coupling between such oscillations and the spontaneous periodic contraction of isolated cardiac myocytes, which would take into account the cell mechanical properties and morphology, is largely lacking.

In the present work, we propose a virtual cardiac cell which exhibits the experimentally observed qualitative and quantitative features of the rhythmic contraction of isolated cardiomyocytes. Starting from the one-pool CICR model proposed by Goldbeter *et al.* (1990), we developed a mechano-chemical cell model, which couples the anisotropic diffusion of Ca^{2+} cytosolic concentrations to the anisotropic contraction of the cell sarcomeres. This coupling is based on a precise quantification of the cardiac cell rheology derived from the stress/strain response curves experimentally obtained with isolated cells (Cazorla *et al.*, 2003). With the aid of the bifurcation diagrams associated with the nonlinear cell model, 2D finite element simulations of the virtual cell deformations have been undertaken and compared to the self-sustained contractions of isolated rat cardiomyocytes recorded by time-lapse video-microscopy.

2. MATERIALS AND METHODS

2.1. Cell Isolation

Cardiac myocytes were kindly provided by the LBFA laboratory (Grenoble University). Briefly, cells were isolated from rat heart ventricles by enzymatic dissociation as described in Olivares *et al.* (1992). Cardiomyocyte contractions were then observed at room temperature to favour spontaneous cell contraction.

2.2. Time-Lapse Video-Microscopy

The spontaneous contractions of the isolated rat cardiomyocytes have been recorded by phase contrast time-lapse videomicroscopy, using an imaging workstation composed of an inverted microscope (Zeiss Axiovert 135) equipped with a Phase 1 Achrostigmat 5x or x10 objective, automated shutters (Uniblitz) and a CCD camera (CoolSNAP, Roper Scientific) monitored via a computer by an image acquisition and analysis software (MetaVue, Roper Scientific). The microscope calibration was performed using a micrometric slide (PRESS-PRO21). Scaling along x and y axes with 5x objective were respectively of 0.833 μm/pixel and 0.909 μm/pixel.

3. DESCRIPTION OF THE MODEL

3.1. Modelling Intracellular Calcium Oscillations

As a first step of our modelling approach, we considered the simplified but quite well established two-variable model of Goldbeter *et al.* (1990) as a basic core for the generation of spontaneous self-sustained calcium oscillations. In this model, the CICR process is described by nonlinear fluxes between cytosolic $Z(t)$ and sarcoplasmic $Y(t)$ calcium concentrations.

In order to take into account spatial effects linked to the intracellular propagation of free calcium within the cardiomyocyte, we extend the above CICR model by considering the anisotropic diffusion of cytosolic calcium. Indeed, using microinjection of a non-reactive fluorophore, Subramanian *et al.* (2001) found experimentally that calcium diffusion in the cytoplasm of cardiac cells is anisotropic, with longitudinal diffusion (i.e. along the principal cell axis) being favoured over transverse diffusion.

Considering a 2D domain corresponding to the projected morphology of an isolated cardiac cell (Figure 1), the spatio-temporal variation of $Z(\mathbf{r}, t)$ and $Y(\mathbf{r}, t)$ at location $\mathbf{r}(x, y)$ within the cell is thus given by the following partial differential equations:

$$\left|\frac{\partial Z}{\partial t} = \nu_0 + \nu_1.\beta - \nu_2(Z) + \nu_3(Y, Z) + k_f.Y - k.Z + \nabla.(\mathbf{D}\nabla Z)\right. \tag{1}$$

$$\left|\frac{\partial Y}{\partial t} = \nu_2(Z) - \nu_3(Y, Z) - k_f.Y\right. \tag{2}$$

In this model, $\nu_1\beta$ is the constant flux of calcium into the cytosol, controlled by the calcium concentration inside the SR as well as by IP_3 concentrations. The flux $k_f Y$ is a basal leak of calcium from the SR, while the input flux ν_0 and efflux kZ refer to the inward and outward Ca^{2+} fluxes taking place at the cell membrane respectively. The intracellular calcium fluxes ν_2 and ν_3 are modelled by enzymatic like Michaelis-Menten reaction terms, where the integers n, m and p represent the cooperativity degrees of the activation process, according to the relationships:

$$\nu_2 = V_{M2}.\frac{Z^n}{K_2^n + Z^n} \quad \nu_3 = V_{M3}.\frac{Y^m}{K_R^m + Y^m}.\frac{Z^p}{K_A^p + Z^p} \tag{3}$$

where the positive constants V_{M2} and V_{M3} define the maximum rates of Ca^{2+} pumped into and released from the SR respectively. $\mathbf{D}$ is a diagonal diffusion tensor with components $D_{ii}(D_{ij} = 0)$. According to experimental data (Subramanian *et al.*, 2001), we

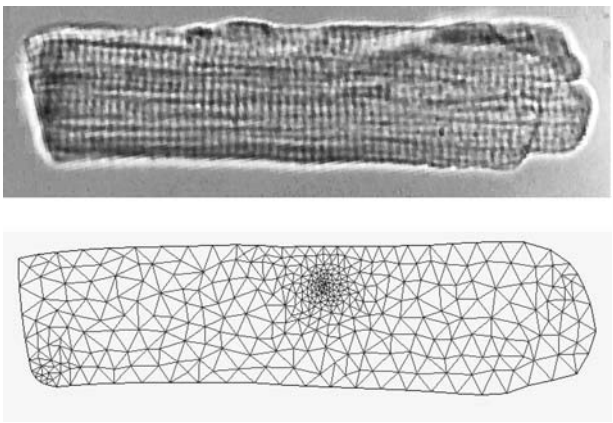

Figure 1. Microscopic view of an isolated rat cardiomyocyte and associated geometrical 2D domain showing the geometrical boundaries and the finite element mesh used in the model simulations. The cell size is of 110 μm $\times$ 27 μm. The spatial mesh is refined in the neighbourhood of the small central region where the cell is assumed to be stuck to the underlying dish. This corresponds to zero displacement boundary conditions in the model.

considered the ratio $\frac{D_{22}}{D_{11}}$ between transverse diffusion coefficient and longitudinal diffusion coefficient to be equal to 0.5.

Equations are non-dimensionnalized, according to the change of variables given in the appendix, with new variables

$$C(\mathbf{r}, \tau) = \frac{Z(\mathbf{r}, t)}{K_2}; \quad S(\mathbf{r}, \tau) = \frac{Y(\mathbf{r}, t)}{K_R} \tag{4}$$

where the vector $\mathbf{r}$ denotes the spatial position and τ is the normalized time.

The spatio-temporal variation of these normalized Ca^{2+} concentrations are then given as solutions of the following nonlinear differential system:

$$\begin{cases} \dfrac{\partial C(\mathbf{r}, \tau)}{\partial \tau} = \varphi - C(\mathbf{r}, \tau) + .\dfrac{k_r}{k_e} fcs[C(\mathbf{r}, \tau), S(\mathbf{r}, \tau)] + \nabla.(\mathbf{d}\nabla C) \\ \dfrac{\partial S}{\partial \tau} = \dfrac{-1}{k_e}.fcs[C(\mathbf{r}, \tau), S(\mathbf{r}, \tau)] \\ C(\mathbf{r}, 0) = C_0; \quad S(\mathbf{r}, 0) = S_0 \end{cases} \tag{5}$$

with

$$fcs(C, S) = k_s.S. + \left(\frac{C^p}{k_a^p + C^p}\right).\left(\frac{S^m}{1 + S^m}\right) - k_{23}(C^n/1 + C^n)\left(\frac{C^n}{1 + C^n}\right) \tag{6}$$

This model can be put into the form of a generalised FitzHugh-Nagumo model for describing excitable membrane (Sneyd *et al.*, 1993; Keener and Sneyd, 1998), which provides a general framework for the analysis of the virtual cell model dynamical properties.

3.2. Modelling Anisotropic Cardiomyocyte Contraction

As recalled in the introduction section, cytosolic calcium concentrations monitor the mechanical contraction of the cardiac cell sarcomeres. This mechanical force is generated by myosin dependent sliding of actin filaments, the overall process being controlled by the local calcium concentrations.

3.2.1. *Passive mechanical properties*

The cellular medium is assumed to be an homogeneous quasi-incompressible and hyperelastic neo-Hookean continuum (Holzapfel, 2001), characterized by a strain-energy function already used to model the mechanical response of tissues and living cells (Caille *et al.*, 2002; Ohayon et Tracqui, 2005) and given by:

$$W = a_1(I_1 - 3) \tag{7}$$

where a_1 is the cellular material constant (in Pa), while I_1 is the first invariant of the right Cauchy-Green strain tensor $\mathbf{C}$ ($I_1 = \text{Trace}(\mathbf{C})$).

For this incompressible medium, the initial shear modulus G is related to the initial Young's modulus E_{cell} by the equation $E_{\text{cell}} = 3\,\text{G}$. Furthermore, an additional explicit relationship between E_{cell} and the material constant a_1 can be obtained for uniaxial tension or compression of the medium: in this case, $E_{\text{cell}} = 2a_1(2 + \lambda^{-3})$ where λ is the extension ratio in the direction of the uniaxial stress. Notice that for small extension ratio ($\lambda \sim 1$), this expression reduces to $E_{\text{cell}} \sim 6a_1$.

3.2.2. *Active contraction model*

In order to incorporate the anisotropic active contraction, an active tension T_{active} is applied along the deformed sarcomere direction, which is specified by the unit vector e_x (Bourdarias *et al.*, 2003). Hence the Cauchy stress tensor in active loaded state is given by:

$$\tau = -pI + F\frac{\partial W}{\partial E}F^T + \tau_{\text{active}} \tag{8}$$

with

$$\tau_{\text{active}} = T_{\text{active}} e_x \otimes e_x \tag{9}$$

where p is the Lagrangian multiplier resulting of the incompressibility condition (i.e. $\det F = 1$), equivalent to an internal pressure. The symbol $\otimes$ denotes the tensor product, and I, F and E are the identity, elastic gradient and Green strain tensors, respectively (Holzapfel, 2001). One can note that the last term of the Equation (8) gives the expression of the active Cauchy stress tensor.

3.2.3. *Coupling active stress with calcium concentrations*

In this study, the local amplitude of the active tension is assumed to be calcium concentration-dependent

$$T_{\text{active}} = \gamma(Z).T_{\max} \tag{10}$$

So, $\gamma(Z).T_{\max}$ represents local active cellular tension driven by the intracellular calcium concentration $Z(r, t)$, and $T_{\max}$ is the maximal tension that can be delivered by

the sarcomere. In agreement with experimental data (Stuyvers *et al.*, 2002), we modelled the mechanical coupling described by the normalized function $\gamma(Z)$ by the Hill function:

$$\gamma(Z(r,t)) = \frac{Z^{n_H}}{Z_{50}^{n_H} + Z^{n_H}} \tag{11}$$

where the positive constant n_H is the Hill coefficient and Z_{50} represents the half-maximum concentration of cytosolic calcium.

Assuming plane strain loading and neglecting inertial effects and volumic forces, the local equilibrium equations are numerically solved using a finite element method (Femlab© software, Comsol) in the 2D domain extracted from real cell morphology (Figure 1).

The following boundary conditions are considered in the simulations: (i) zero-fluxes (Neumann) conditions for $Z(\mathbf{r}, t)$ and $Y(\mathbf{r}, t)$ on the cell boundaries (ii) zero displacement conditions at the cell centre and (iii) stress free boundary conditions on the cell boundaries ($\sigma . \mathbf{n} = 0$, where $\mathbf{n}$ is the vector normal to the cell membrane).

4. RESULTS

4.1. Existence of Time-Periodic Solutions of the Model

The temporal dynamics of the model has been analyzed with the continuation algorithms provided in the software package MATCONT (Dhooge *et al.*, 2003). Generation of periodic solutions from bifurcations of the steady-states is illustrated in Figure (2A). On the right-side of the bifurcation diagram, a stable limit cycle bifurcates from the steady-state by a Hopf bifurcation. A second Hopf bifurcation is located on the left side of the diagram, occuring for small values of the model parameter β in this case, the emerging limit-cycle is unstable. The Hopf bifurcation is sub-critical and a stable periodic limit cycle appears for a lower value of parameter β through a saddle-node bifurcation of periodic orbits.

The corresponding evolution of the period of the calcium oscillations is given in Figure (2B). Model parameters have been chosen accordingly in order to get a period of the order of 20 sec.

4.2. Identification of Cell Mechanical Properties

From the experimental measurements of Cazorla *et al.* (2003), we estimated a secant Young's modulus of about 30 kPa. Taking into account this elastic modulus value, we furthermore assumed that the homogenised cardiomyocyte behaves like a nearly incompressible medium.

4.3. Quantification of the Cell Contraction Dynamics

Typical snapshots of a cardiomyocyte contraction/relaxation dynamics are presented in Figure 3. This images acquisition procedure enables us to first, establish the periodicity of the cell contraction, second to quantify the contraction period and amplitude, the duration of the non contracting phase as well as the cell contraction time profile (Table 1). This overall dynamical pattern will be compared to our simulated cell behaviour.

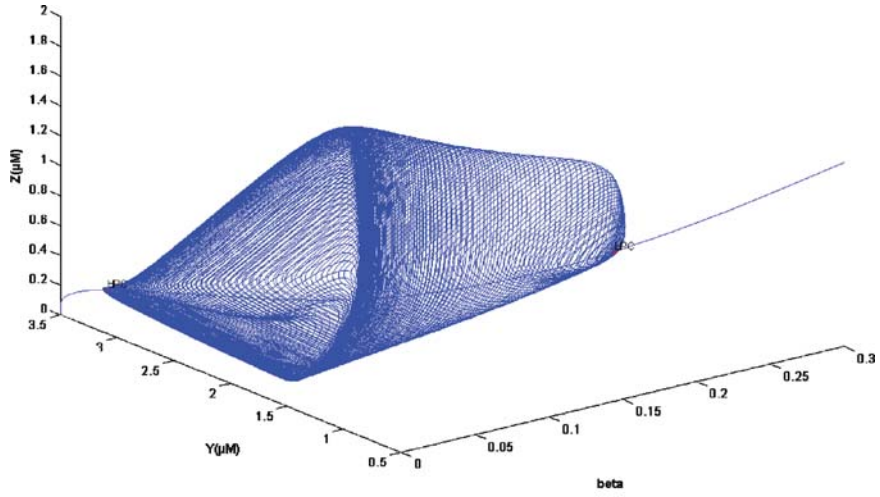

A

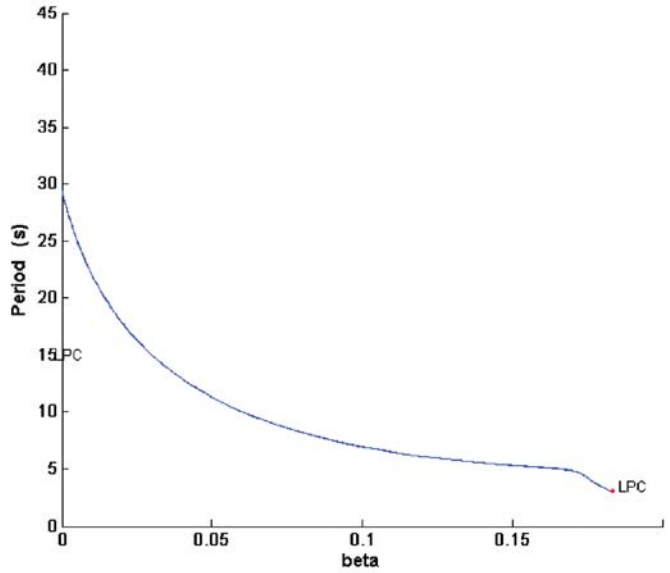

B

Figure 2. Bifurcation diagram given by the nonlinear model of intracellular temporal calcium oscillations associated with the differential system (1–2). Parameter β, which controls the balance of calcium fluxes from the IP_3 sensitive pool and from the extracellular medium, has been chosen as a bifurcation parameter. (A) Evolution of the limit cycle in the phase plane $(Y(t), Z(t))$ when β increases and goes through successively sub-critical and super-critical Hopf bifurcation points. (B) Associated variation of the period of the limit cycle.

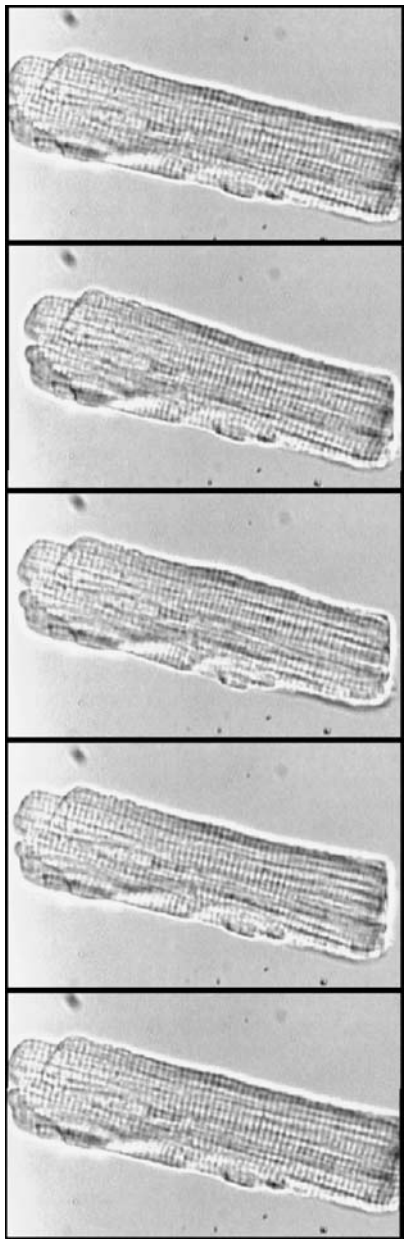

Figure 3. Time-lapse sequence, recorded by phase-contrast video-microscopy, showing the spontaneous contraction of an isolated rat cardiomyocyte. Contraction starts on the bottom part of the image, and then propagates to the upper part before a complete relaxation back to the inactivated state of the cell. If time is set to zero for the first image on the left, successive times when browsing the image sequence from left to right are respectively: 0.2 s – 0.5 s – 0.8 s – 1.4 s.

Table 1. Quantification of the main features of the periodic spontaneous contraction we experimentally observed with isolated rat cardiomyocytes. These values are derived from the analysis of the series of time-lapse videomicroscopy image sequences we recorded on 6 contracting cells taken randomly in the dish

Number of cells	Contraction period	Duration of the resting phase	Contraction duration	Contraction amplitude
6	17.0 ± 5.8 s	15.5 ± 5.4 s	1.5 ± 0.4 s	$8 \pm 0.9\,\mu$ m

Typically, the cell contraction periodicity is around 17 sec, including a very brief cell contraction phase (1.5 sec) followed by a rest phase lasting almost 15.5 sec. (Table 1). The maximal contraction amplitude of the cardiac cell is about 7.3% corresponding approximately to 8 μm.

4.4. Simulating Virtual Cardiac Cell Contraction

On the basis of the theoretical analysis and on experimental data, the kinetic parameters defining the different calcium fluxes have been adjusted in order to get a simulated temporal pattern of cardiomyocyte contraction which quantitatively agrees with the recorded videomicroscopy time-lapse sequences. Their values are summarized in Table 2. We also derived the amplitude $T_{\max}$ of the active stress σ_{active}. We get a value of 3 kPa in order to obtain a contraction amplitude of about 8 μm ($\sim$7% of cell length), which is the mean value we obtained from the analysis of time-lapse sequences (Table 1). The resulting time sequences of simulated cells morphological changes are presented in figures 4 and 5.

The concentrations of free cytosolic calcium $Z(t)$ oscillate between low values, during which calcium is pumped into the SR (ν_2 flux), and high values resulting from autocatalytic efflux ν_3 of calcium released by the SR.

The finite element simulations of cardiomyocyte contraction compare very satisfactorily with the observed real cellular dynamics. Assuming that a localized increase of cytosolic calcium concentration occured on the left side of the cell, we observed the subsequent propagation of a contraction wave from left to right (Figure 5), associated with localized increasing then decreasing cellular deformations (Figure 6).

Figure 4 shows that the simulated contraction/relaxation appears periodically every 16.6 sec and lasts approximately 3 sec, which agrees rather well with the mean experimental values we measured (Table 1).

Figure 7 illustrates the temporal evolution of the Von Mises stresses, which reveals the coupling between chemical and mechanical cell dynamics. Maximum stress values propagate from left to right, keeping the cell under stress during all the propagation of the calcium wave. Interestingly, the cell remains almost homogeneously contracted during a short period, thus delivering at this time its maximal contractility performance.

5. DISCUSSION

Considering simultaneously a minimal nonlinear model of intracellular oscillations and experimentally based cardiac cell mechanical properties, we propose in this work an

Table 2. Set of biochemical and biomechanical parameter values used for the virtual cardiomyocyte simulations. Most of the biochemical parameters values are taken from the original validation provided in Goldbeter *et al.* (1990)

Model parameters	Definition	Values	Units
	Biochemical parameters		
υ_0	Basal Ca^{2+} influx from extracellular medium, assumed constant	0.33	$\mu M.s^{-1}$
k	Rate of passive Ca^{2+}efflux from cytosol to extracellular medium	1.0	s^{-1}
k_f	Rate of passive Ca^{2+}efflux from SR into cytosol	0.1	s^{-1}
υ_1	Stimulated Ca^{2+} influx from extracellular medium, space dependant	2.3	$\mu M.s^{-1}$
β		0.1	–
V_{M2}	Maximal rate of Ca^{2+} uptake into SR	8.0	$\mu M.s^{-1}$
K_2	Threshold constant for Ca^{2+} uptake into SR	1.0	μM
V_{M3}	Maximal rate of CICR from SR	45.5	$\mu M.s^{-1}$
K_A	Threshold constant for CICR from SR	0.93	μM
K_R	Threshold constant for Ca^{2+}release from SR	2.0	μM
n	Hill exponent of Ca^{2+}uptake into SR	2	
m	Hill exponent of Ca^{2+}release from SR	2	
p	Hill exponent of CICR from SR	4	
Y_0	Model steady-state Ca^{2+}concentration in SR	0.1	μM
Z_0	Model steady-state concentration of cytosolic Ca^{2+}	1.6	μM
	Spatial parameters		
D_{11}	Longitudinal Ca^{2+}diffusion coefficient	100	$\mu m^2.s^{-1}$
D_{22}	Transverse Ca^{2+}diffusion coefficient	50	$\mu m^2.s^{-1}$
$D_{12,}\, D_{21}$	Cross-correlated Ca^{2+}diffusion coefficients	0	$\mu m^2.s^{-1}$
	Biomechanical parameters		
a_1	Cardiomyocyte elasticity modulus	5	kPa
$T_{\max}$	Cardiomyocyte contractile tone	3	kPa
n_H	Hill coefficient for Ca^{2+}dependant contraction	4	
Z_{50}	Half-maximal concentration value for Ca^{2+}dependant contraction	3.0	μM

original model of isolated cardiomyocyte periodic and self-sustained contractions. The virtual cardiomyocyte dynamics compare very satisfactorily with real time-lapse videomicroscopy sequences. This agreement is obtained both qualitatively and quantitatively, with simulated cell contraction period, duration and amplitude quite close to the measured experimental values.

However, some limitations of the present model deserve to be discussed. The first one concerns the passive rheological properties of the cardiomyocyte. Indeed, we assumed linear and isotropic elasticity, while the stress elongation response curve is nonlinear.

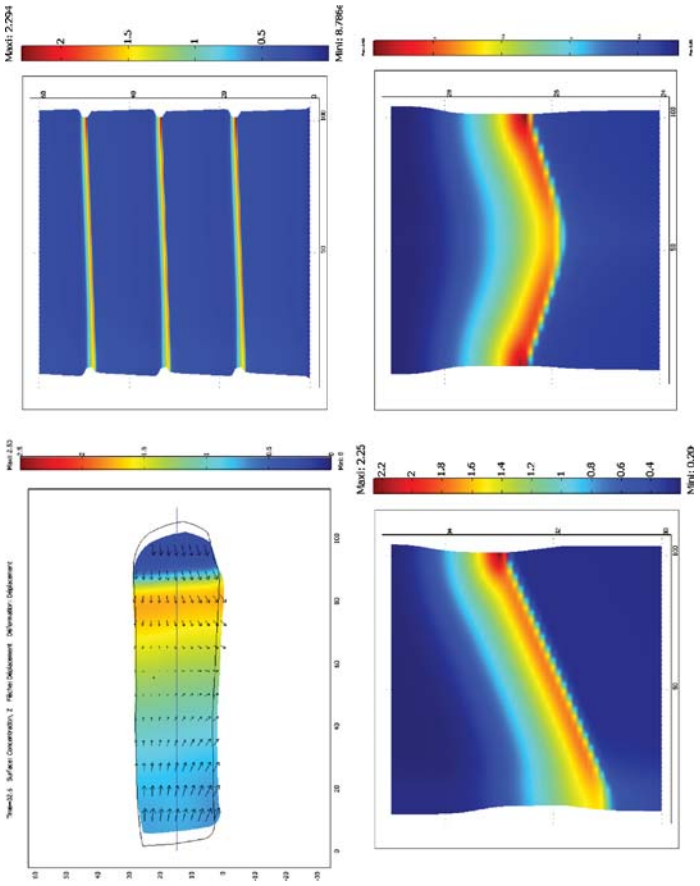

Figure 4. Simulated line scan observation of the cytosolic concentrations $Z(t, x, y)$ during repeated cardiomyocyte contractions. Upper left: location of the line scan along the cell ($y = 15$ μm) and simulated displacement field obtained when maximum $Z(t, x, y)$ values are located just after the middle of the cell. Upper right: Simulated values $Z(t, x, y = 15)$ along the line scan when time (vertical axis) increases from 0 to 60 s. Each yellow (or light grey) oblique line corresponds to a cell contraction. The longitudinal displacement u has been superimposed to the x-axis in order to indicate the amplitude of the contraction. The periodicity of the contraction is of 16.7s. Lower left: enlargement of the upper right figure on the time interval [30s, 35s] during which one contraction propagates from the left to the right side of the cell. Lower right: similar enlargement obtained when the contraction has been initiated in the centre of the cell. The calcium wave and associated contraction now propagates from the centre to both ends of the cell.

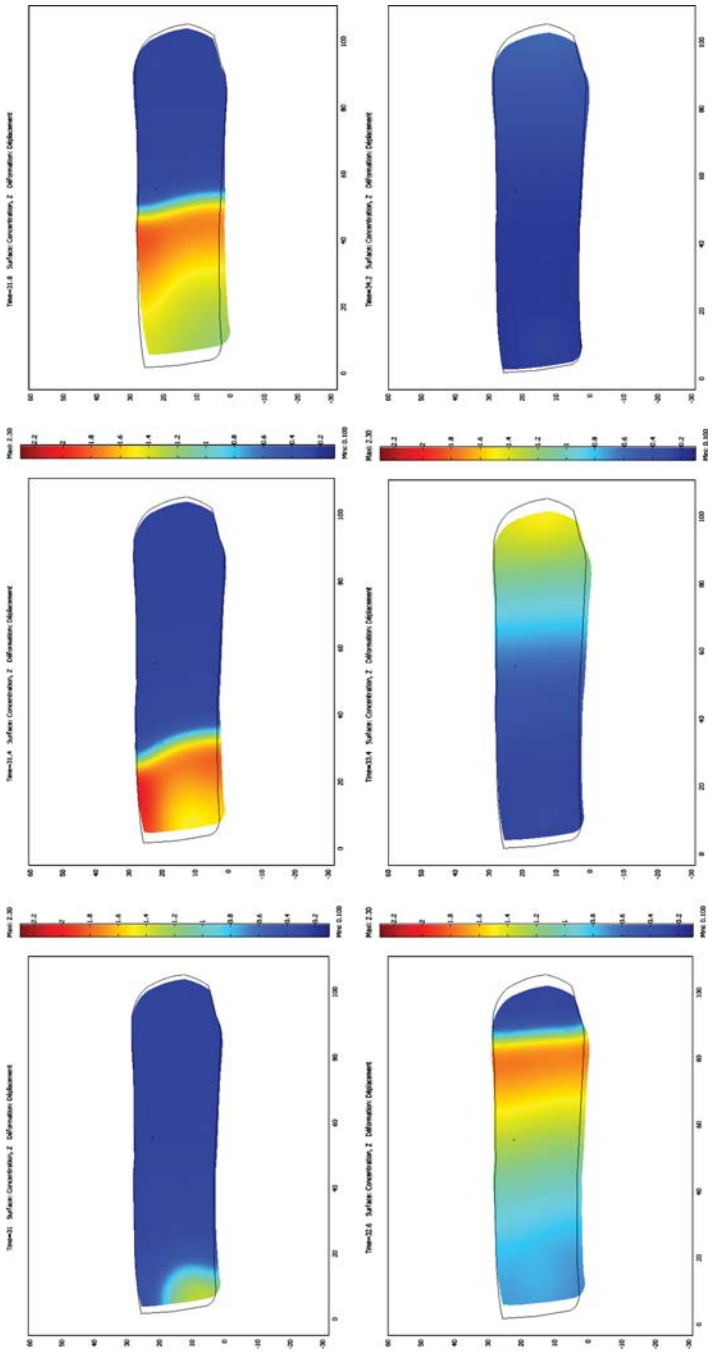

Figure 5. Finite element simulation of the calcium wave propagation initiated by a spark-like domain located on the lower left part of the cell. The sequence of images shows the motion of high $Z(t, x, y)$ values (green-red (or light grey) band) as a soliton driving the cell contraction up to the cell mechanical relaxation (last image). The amplitude of the contraction is indicated by reference to the cell boundaries in the relaxed state (thin solid lines). Simulation times, from left to right and from top to bottom are respectively: 31s; 31.4s; 31.8s; 32.6s; 33.4s; 34.2s.

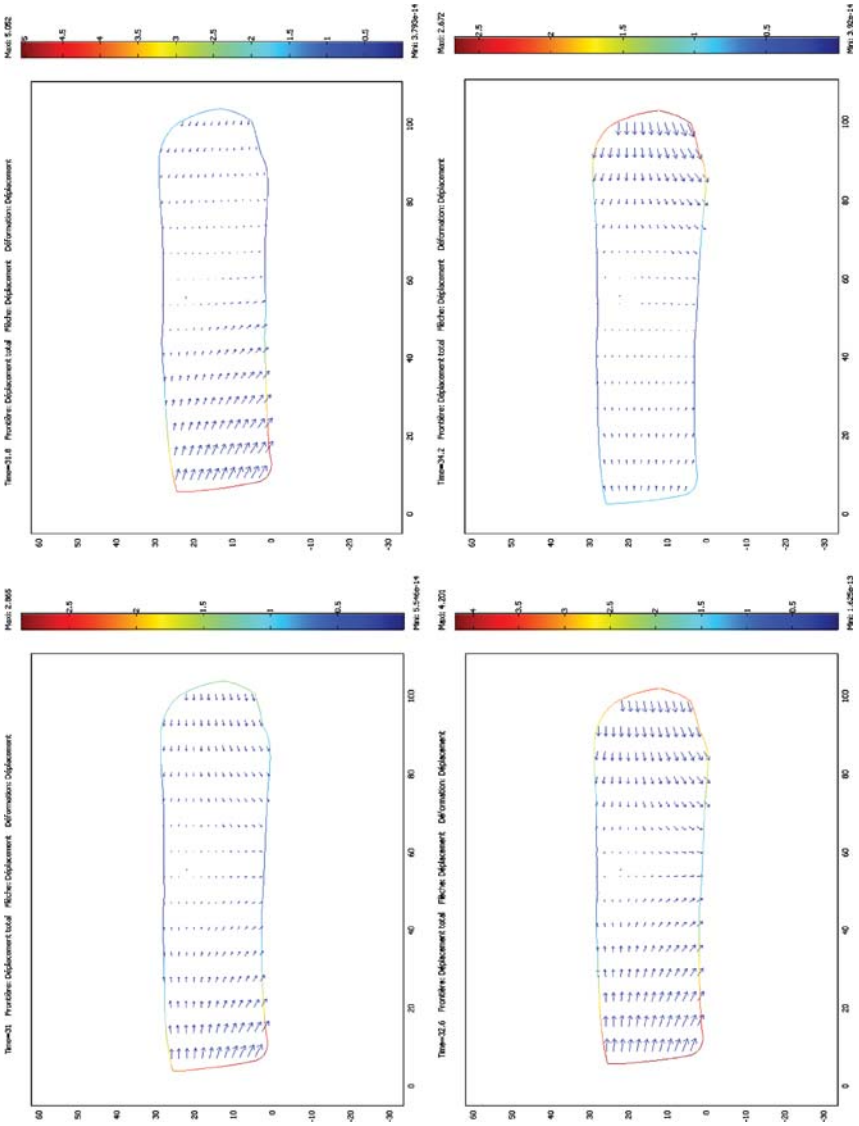

Figure 6. Associated displacement vector fields corresponding to the simulated cell contraction observed at times 31 s; 31.8 s; 32.6 s and 34.2 s in Figure 5.

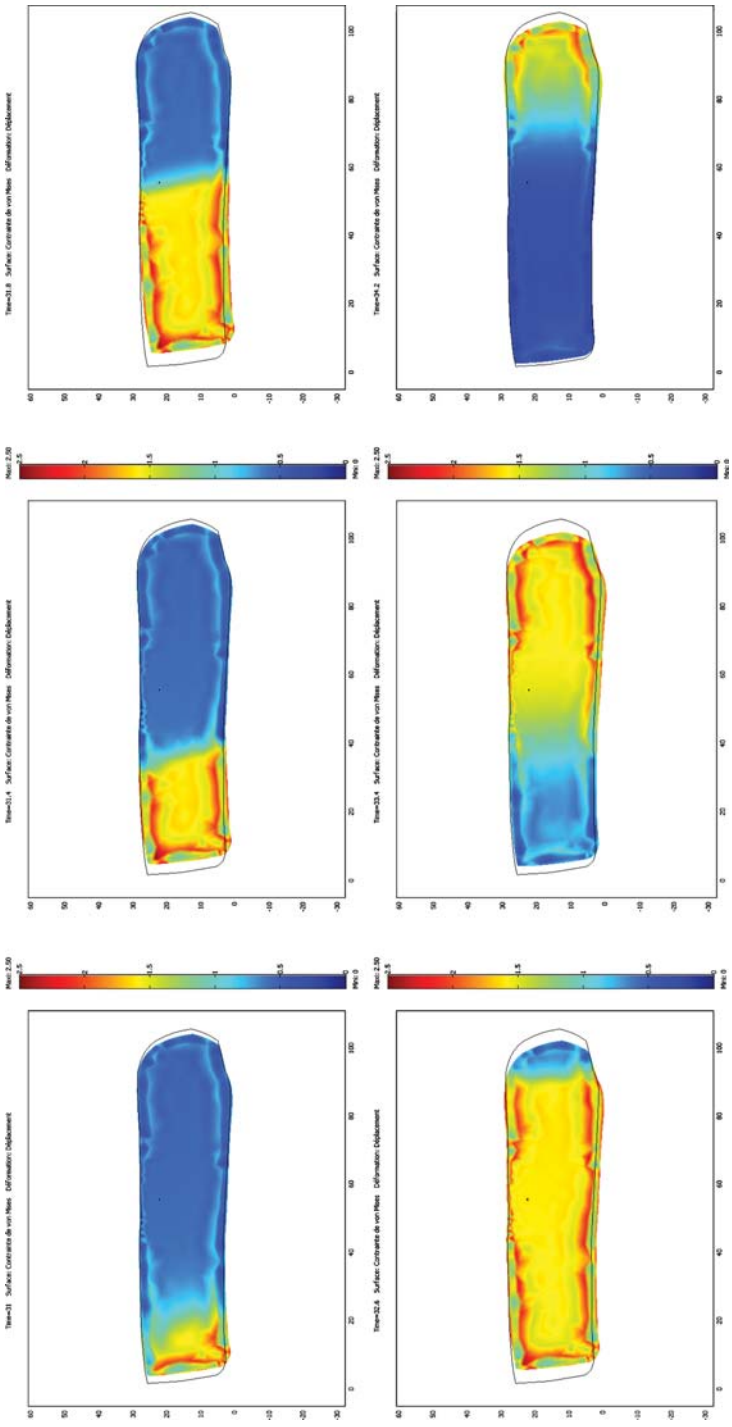

Figure 7. Spatio-temporal evolution of the intracellular stresses (Von Mises stresses) within the cardiomyocyte as the calcium wave propagates within the cell. The time sequence is the same as the one used in Figure 5. Thus, each stress map can be associated with the corresponding cytosolic calcium distribution shown in Figure 5. One can notice that at time 32.6 s, all the cell body is under tension.

Another limitation is due to the plane strain hypothesis we used: the cell anisotropy and almost cylindrical shape of cardiomyocytes tends to support plane stress conditions.

Even if a detailed presentation of all biochemical and biomechanical processes would require more detailed models, the present work underlines how such an *in silico* approach can help to integrate data and dynamical cell properties on both calcium kinetics, cell rheological parameters and calcium/stress relationships. In the context of computational biology, this study thus provides a reliable basis for further investigations of the different mechanotransduction pathways activated by mechanical stretches within cardiac myocytes through an explicit consideration of the coupling between cell stretching and intracellular calcium dynamics.

ACKNOWLEDGEMENTS

We thank Dr. A. Lacampagne (INSERM, Montpellier, France) for rheological data and Dr. J. Olivares (LBFA-UJF, Grenoble, France) for providing isolated cardiomyocytes. This work was supported by grants from Inst. Math. Appl. Grenoble (IMAG) (CatiMy project) from CNRS (MoCeMy project) and European 6th call (CRAFT project Disheart).

APPENDIX

The calcium model is defined by the nonlinear differential system:

$$\begin{cases} \dfrac{\partial Z}{\partial t} = \nu_0 + \nu_1.\beta - V_{M2}\dfrac{Z^n}{K_2 + Z^n} + V_{M3}\dfrac{Z^p}{K_A^p + Z^p}\dfrac{Y^m}{K_R^m + Y^m} \\ \qquad\qquad + k_f.Y - k.Z + \nabla.(\mathbf{D}\nabla Z) \\ \dfrac{\partial Y}{\partial t} = V_{M2}\dfrac{Z^n}{K_2 + Z^n} - V_{M3}\dfrac{Z^p}{K_A^p + Z^p}\dfrac{Y^m}{K_R^m + Y^m} - k_f.Y \end{cases} \tag{A.1}$$

Equations are non dimensionalized according to the following change of variables:

$$\begin{gathered} C(\mathbf{r},\tau) = \frac{Z}{K_2} \quad S(\mathbf{r},\tau) = \frac{Y}{K_R} \quad k_a = \frac{K_A}{K_2} \quad k_{23} = \frac{V_{M2}}{V_{M3}} \quad k_r = \frac{K_R}{K_2} \\ k_s = \frac{k_f.K_R}{V_{M3}} \quad k_e = \frac{k.K_R}{V_{M3}} \quad \varphi = \frac{\nu_0 + \nu_1.\beta}{k.K_2} \quad d\tau = k.\,dt \quad \mathbf{d} = \frac{1}{k}\mathbf{D} \end{gathered} \tag{A.2}$$

One then gets the nonlinear differential system governing the normalized Ca^{2+} concentration of in the cytosol and the SR, denotes $C(\mathbf{r},\tau)$ and $S(\mathbf{r},\tau)$ respectively:

$$\begin{cases} \dfrac{\partial C(\mathbf{r},\tau)}{\partial \tau} = \varphi - C(\mathbf{r},\tau) + .\dfrac{k_r}{k_e} fcs\,[C(\mathbf{r},\tau), \quad S(\mathbf{r},\tau)]\,\tau = \nabla.(\mathbf{d}\nabla C) \\ \dfrac{\partial S}{\partial \tau} = \dfrac{-1}{k_e}.fcs\,[C(\mathbf{r},\tau), S(\mathbf{r},\tau)] \end{cases} \tag{A.3}$$

with

$$fcs(C,S) = k_s.S. + \left(\frac{Q^p}{k_a^p + Q^p}\right).\left(\frac{S^m}{1+S^m}\right) - \left(\frac{Q^n}{1+Q^n}\right) \tag{A.4}$$

REFERENCES

Bourdarias, C., S. Gerbi and J. Ohayon (2003). A three dimensional finite element method for biological active soft tissue-Formulation in cylindrical polar coordinates. Mathematical Modelling and Numerical Analysis 37(4): 725–739.

Caille, N., O. Thoumine, Y. Tardy and J.J. Meister (2002). Contribution of the nucleus to the mechanical properties of endothelial cells. Journal of Biomechanics 35: 177–187.

Cazorla, O., A. Lacampagne, J. Fauconnier and G. Vassort (2003). SR 33805 a Ca^{2+} antagonist with length-dependent Ca^{2+}-sensitizing properties in cardiac myocytes. British Journal of Pharmacology 139: 99–108.

Dhooge, A., W. Govaerts and Yu, A. Kuznetsov (2003). MATCONT: A MATLAB package for numerical bifurcation analysis of ODEs. ACM Transactions in mathematical software 29: 141–164.

Fabiato, A. (1983). Calcium-induced release of calcium from the cardiac sarcoplasmic reticulum, American Journal of Physiology 245: C1–C14.

Fabiato, A. and F. Fabiato (1975). Contraction induced by a calcium-triggered release of calcium from the sarcoplasmic reticulum of single skinned cardiac cell. Journal of Physiology London 249: 469–495.

Goldbeter, A., G. Dupont and M.J. Berridge (1990). Minimal model for signal-induced Ca^{2+} oscillations and for their frequency encoding through protein phosphorylation. Proceedings of the National Academy of Sciences, USA 87: 1461–1465.

Grouselle, M., B. Stuyvers, S. Bonoron-Adele, P. Besse and D. Georges-Cauld (1991). Digital imaging microscopy analysis of calcium release from sarcoplasmic reticulum in single rat cardiac myocytes. Pfluegers Archives 418: 109–119.

Holzapfel, G.A. (2001). Nonlinear Solid Mechanics. Ed. Wiley & Sons, NY.

Ishida, H., C. Genka, Y. Hirota, H. Nakazawa and W.H. Barry (1999). Formation of planar and spiral Ca^{2+} waves in isolated cardiac myocytes Biophysical Journal 77: 2114–2122

Keener, J. and J. Sneyd (1998). Mathematical Physiology, Springer Verlag. NewYork.

Lakatta, E. (1992). Functional implications of spontaneous sarcoplasmic reticulum Ca^{2+} release in the heart. Cardiovascular Research 26: 193–214.

Ohayon, J. and P. Tracqui (2005). An extended method for computing the apparent stiffness of individual cell probed by magnetic twisting cytometry. Annals of Biomedical Engineering 33(2): 131–141.

Olivares, J., I. Dubus, A. Barrieux, J.L. Samuel, L. Rappaport and A. Rossi (1992). Pyrimidine nucleotide synthesis is preferentially supplied by exogenous cytidine in adult rat cultured cardiomyocytes. Journal of Molecular and Cellular Cardiology 24: 1349–1359.

Slepchenko, B.M., J.C. Schaff, I. Macara and L.M. Loew (2003). Quantitative cell biology with the Virtual Cell. Trends in Cell Biology 13: 570–576.

Sneyd, J., S. Girard and D. Clapham (1993). Calcium wave propagation by calcium-induced calcium release: An unusuable excitable system. Bulletin of Mathematical Biology 55: 315–344.

Stern, M.D., M.C. Capogrossi and E.G. Lakatta (1988). Spontaneous calcium release from the sarcoplasmic reticulum in myocardial cells: Mechanisms and consequences. Cell Calcium 9: 247–256.

Stuyvers, B.D, A.D. McCulloch, J. Guo, H.J. Duff and H.E.D.J. ter Keurs (2002). Effect of stimulation rate, sarcomere length and Ca^{2+} on force generation by mouse cardiac muscle. Journal of Physiology 544(3): 817–830.

Subramanian, S., S. Viatchenko-Karpinski, V. Lukyanenko, S. Györk and T.F. Wiesner (2001). Underlying mechanisms of symmetric calcium wave propagation in rat ventricular myocytes. Biophysical. Journal 80: 1–11.

Takamatsu, T. and W. Wier (1990). Calcium waves in mammalian heart: Quantification of origin, magnitude, waveform and velocity. FASEB Journal 4: 1519–1525.